Elasticity of Fractal Inspired Interconnects

*Yewang Su, Shuodao Wang, YongAn Huang, Haiwen Luan, Wentao Dong, Jonathan A. Fan, Qinglin Yang, John A. Rogers, and Yonggang Huang**

The use of fractal-inspired geometric designs in electrical interconnects represents an important approach to simultaneously achieve large stretchability and high aerial coverage of active devices for stretchable electronics. The elastic stiffness of fractal interconnects is determined analytically in this paper. Specifically, the elastic energy and the tensile stiffness for an order n fractal interconnect of arbitrary shape are obtained, and are verified by the finite element analysis and experiments.

1. Introduction

Stretchable electronics[1–3] is a field of technology that has recently attracted much research interest, partly due to its wide-ranging prospects for applications, from sensory skins for robotics,[4] to photovoltaics,[5,6] wearable communication devices,[7] transient energy harvester,[8] and other systems that require lightweight, rugged construction in thin, conformal formats,[9] to bio-integrated devices for surgical and diagnostic implements that naturally integrate with the human body to provide advanced therapeutic capabilities,[10] and further to cameras that use biologically inspired designs to achieve superior performance.[11] Success of stretchable electronics depends on the availability of electronic materials and structures (such as the shape of serpentine interconnects and transition area of island-interconnect[12]) that can be highly bent, stretched, compressed and twisted,[13,14] in one-time stretching and cyclic stretching conditions.[15]

One challenge in the development of stretchable electronics is to achieve large stretchability[16,17] without significantly sacrificing the aereal coverage of active devices. Fractal-inspired geometric designs for electrical interconnects between islands of active devices provides an effective approach, with demonstrated utility in stretchable lithium-ion batteries,[18] epidermal electronics and radio frequency antennas.[19] **Figure 1** illustrates zigzag, sinusoidal and serpentine shapes, produced using a fractal design approach.

This paper determines analytically the elasticity of fractal-inspired interconnects. For an order-*n* fractal interconnect of arbitrary shape, the tensile stiffness is obtained analytically in Section 2. The key parameters governing the tensile stiffness are clearly identified. Experiments are carried out to verify the elastic stiffness for the order-2 fractal interconnects, and the results are shown in section 3.

2. Elastic Analysis of Fractal Interconnects

Figure 2a shows an order-*n* fractal interconnect. At each fractal order the interconnect has the same, centrosymmetric

Y. Su, Y. Huang, H. Luan, Prof. Y. Huang
Department of Civil and Environmental Engineering
Northwestern University
Evanston, Illinois 60208, USA
E-mail: y-huang@northwestern.edu
Y. Su, Y. Huang, Prof. Y. Huang
Department of Mechanical Engineering
Center for Engineering and Health
Skin Disease Research Center
Northwestern University
Evanston, Illinois 60208, USA
Y. Su
Center for Mechanics and Materials
Tsinghua University
Beijing 100084, China
S. Wang, Q. Yang, J. A. Rogers
Department of Materials Science and Engineering
Frederick Seitz Materials Research Laboratory University of Illinois at Urbana-Champaign
Urbana, Illinois 61801, USA
Y. Huang, W. Dong
State Key Lab Digital Manufacturing Equipment and Technology
Huazhong University of Science and Technology
Wuhan, Hubei 430074, China
J. A. Fan
Department of Electrical Engineering
Ginzton Laboratory, 348 Via Pueblo Mall
Stanford University
Stanford, CA 94305, USA

DOI: 10.1002/smll.201401181

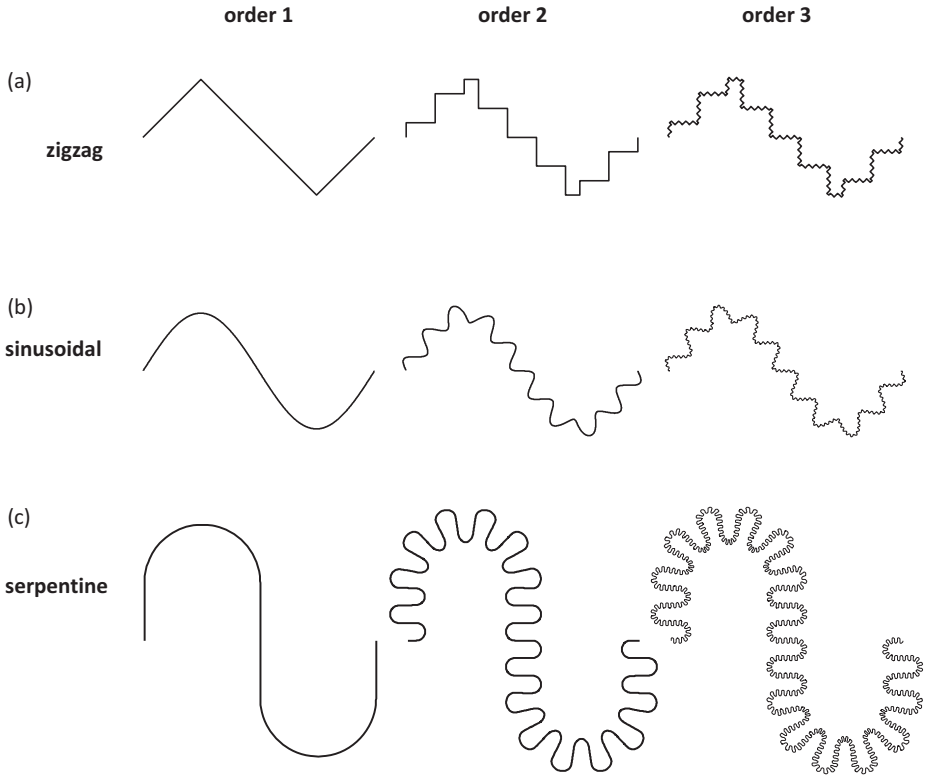

Figure 1. Schematic illustrations of the order-1, 2 and 3 fractal interconnects with the zigzag, sinusoidal and serpentine shapes.

shape, but the size increases by a factor η as the fractal order increases by 1. Figure 2b shows a representative order-1 element, and its shape is described by the local Cartesian coordinates (X,Y) (Figure 2b)

$$X = X(S_1),\ Y = Y(S_1), \tag{1}$$

where the origin of (X,Y) is at the center of this centrosymmetric structure; the curvilinear coordinate S_1 is along the arc length of the order-1 structure, with S_1 = 0 at the center of antisymmetry (Figure 2b) such that $X(-S_1) = -X(S_1)$ and $Y(-S_1) = -Y(S_1)$. The apparent length of the representative element (Figure 2b) is $L_1 = X(S_{1t}/2) - X(-S_{1t}/2) = 2X(S_{1t}/2)$, where S_{1t} is the total length of the representative element. At the two ends of the representative element $Y(-S_{1t}/2) = -Y(S_{1t}/2) = 0$.

The order-1 fractal interconnect is modeled as a beam. Figure 2c shows the sign convention for the positive internal axial force P, shear force Q and bending moment M. Let P_1 and Q_1 denote the internal forces along the local coordinates X and Y, respectively, at the center S_1 = 0, and M_1 bending moment for the order-1 structure (Figure 2b.). The axial and shear forces and bending moment (at any S_1) are then obtained from force equilibrium as

$$\begin{aligned} M(S_1) &= M_1 + P_1 Y(S_1) - Q_1 X(S_1) \\ P(S_1) &= P_1 X'(S_1) + Q_1 Y'(S_1) \\ Q(S_1) &= -P_1 Y'(S_1) + Q_1 X'(S_1), \end{aligned} \tag{2}$$

where $X'(S_1) = dX(S_1)/dS_1$ and $Y'(S_1) = dY(S_1)/dS_1$. The membrane energy is negligible as compared to the bending energy such that the energy density is dominated by the bending energy per apparent length and is given by

$$\begin{aligned} U_1(M_1,P_1,Q_1) &= \frac{1}{L_1}\frac{1}{2EI}\int_{-S_{1t}/2}^{S_{1t}/2}\left[M(S_1)\right]^2 dS_1 \\ &= \frac{1}{EIL_1}\int_0^{S_{1t}/2}\left[M(S_1)\right]^2 dS_1, \end{aligned} \tag{3}$$

where EI is the bending stiffness of the order-1 fractal interconnect. Substitution of Equation (2) into Equation (3) gives the energy density

$$\begin{aligned} &U_1(M_1,P_1,Q_1) \\ &= \frac{1}{2EI}\left[\beta_1 M_1^2 + \beta_2 (P_1 L_1)^2 + \beta_3 (Q_1 L_1)^2\right. \\ &\left. + \beta_4 (P_1 L_1)(Q_1 L_1)\right], \end{aligned} \tag{4}$$

where

$$\begin{aligned} &\beta_1 = \frac{S_{1t}}{L_1},\ \beta_2 = \frac{2}{L_1^3}\int_0^{S_{1t}/2}\left[Y(S_1)\right]^2 dS_1, \\ &\beta_3 = \frac{2}{L_1^3}\int_0^{S_{1t}/2}\left[X(S_1)\right]^2 dS_1, \\ &\beta_4 = \frac{-4}{L_1^3}\int_0^{S_{1t}/2} X(S_1)Y(S_1)\,dS_1 \end{aligned} \tag{5}$$

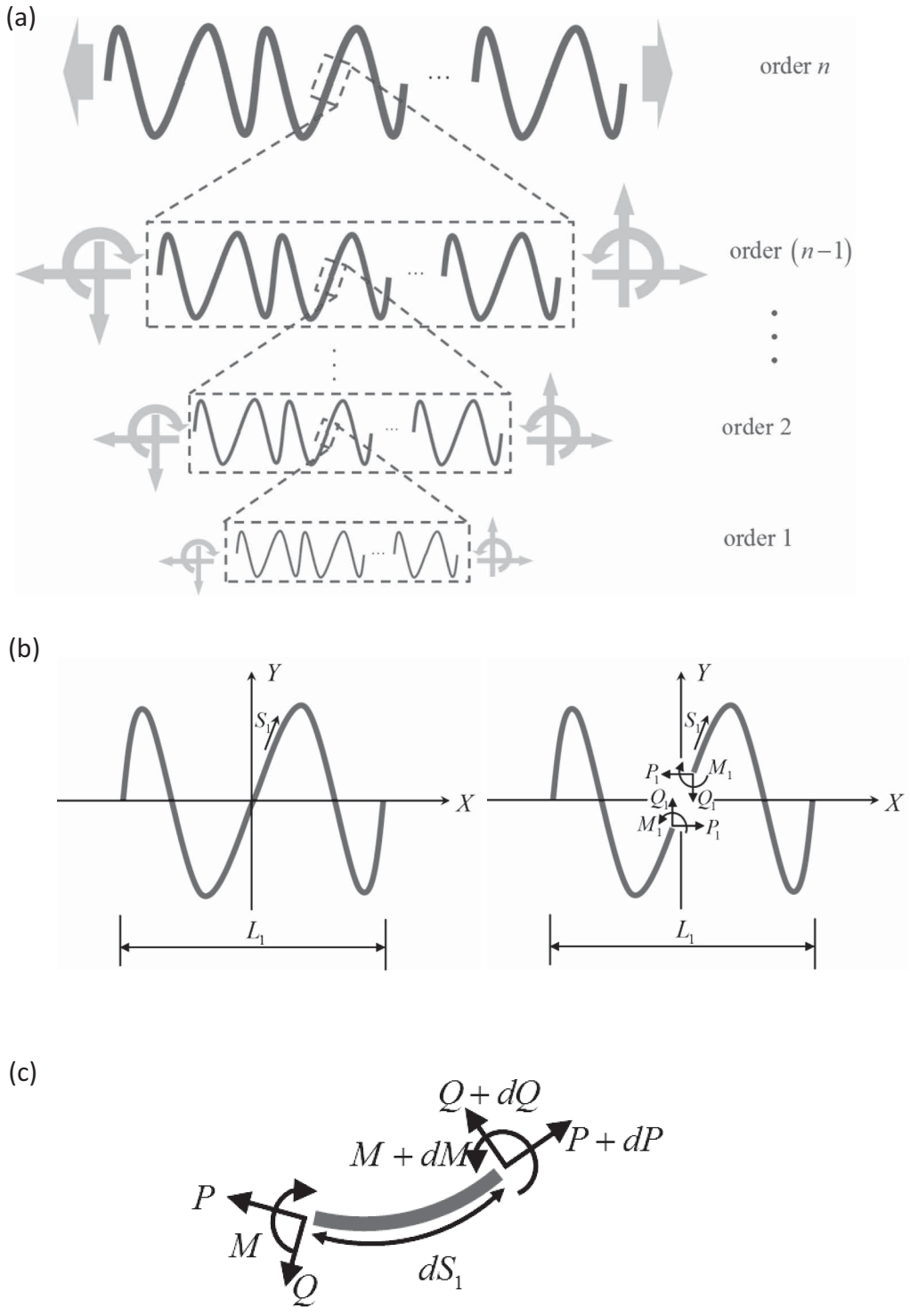

Figure 2. (a) Schematic illustrations of the fractal interconnects with any centrosymmetric shape in a representative element; (b) the curvilinear coordinate S_1 along the arc length and the internal forces P_1 and Q_1 and bending moment M_1 at the center $S_1 = 0$ for the order-1 structure; (c) the sign convention for the internal axial force P, shear force Q and bending moment M.

are dimensionless parameters that depend only on the shape of the order-1 structure, not on its size, and β_1 represents the ratio of total length to the apparent length.

The shape of the order-n is the same as that of the order-1, and therefore is represented by $X = X(S_n)$ and $Y = Y(S_n)$ in its local coordinate, where S_n is the curvilinear coordinate along the arc length of the order-n structure, and the functions X and Y are the same as those in Equation (1). Let P_n and Q_n denote the internal forces along the local coordinates and M_n bending moment at the center $S_n = 0$. Similar to Equation (4), the energy density for the order-n can be generally written as

$$U_n(M_n,P_n,Q_n) = \frac{1}{2EI}\left[\alpha_1^{(n)}M_n^2+\alpha_2^{(n)}(P_nL_n)^2+\alpha_3^{(n)}(Q_nL_n)^2 + \alpha_4^{(n)}(P_nL_n)(Q_nL_n)\right], \quad (6)$$

where the apparent length L_n for order n is related to L_1 for order 1 by $L_n=\eta^{n-1}L_1$, the dimensionless coefficients $\alpha_i^{(n)}$ (i = 1,2,3,4) are to be determined, and $\alpha_i^{(1)}=\beta_i$. The axial force, shear force and bending moment in the order-n structure are actually the internal forces P_{n-1} and Q_{n-1} and bending moment M_{n-1} at the center (S_{n-1} = 0) for order n-1. Similar to Equation (2), force equilibrium then gives

$$\begin{aligned} M_{n-1} &= M_n + P_nY(S_n) - Q_nX(S_n) \\ P_{n-1} &= P_nX'(S_n) + Q_nY'(S_n) \\ Q_{n-1} &= -P_nY'(S_n) + Q_nX'(S_n). \end{aligned} \quad (7)$$

The energy density for order n is the integration of that of the order n–1,

$$U_n(M_n,P_n,Q_n) = \frac{1}{L_n}\int_{-S_{nt}/2}^{S_{nt}/2} U_{n-1}(M_{n-1},P_{n-1},Q_{n-1})dS_n, \quad (8)$$

where $S_{nt}=\eta^{n-1}S_{1t}$. Substitution of Equations (6) and (7) into Equation (8) gives the recursive relation

$$\begin{Bmatrix} \alpha_1^{(n)} \\ \alpha_2^{(n)} \\ \alpha_3^{(n)} \\ \alpha_4^{(n)} \end{Bmatrix} = \begin{Bmatrix} \beta_1 & 0 & 0 & 0 \\ \beta_2 & (\beta_1-\beta_5)/\eta^2 & \beta_5/\eta^2 & -\beta_6/\eta^2 \\ \beta_3 & \beta_5/\eta^2 & (\beta_1-\beta_5)/\eta^2 & \beta_6/\eta^2 \\ \beta_4 & 2\beta_6/\eta^2 & -2\beta_6/\eta^2 & (\beta_1-2\beta_5)/\eta^2 \end{Bmatrix} \begin{Bmatrix} \alpha_1^{(n-1)} \\ \alpha_2^{(n-1)} \\ \alpha_3^{(n-1)} \\ \alpha_4^{(n-1)} \end{Bmatrix}, \quad (9)$$

where the additional dimensionless shape parameters are

$$\begin{aligned} \beta_5 &= \frac{2}{L_1}\int_0^{S_{1t}/2}\left[Y'(S_1)\right]^2 dS_1, \\ \beta_6 &= \frac{2}{L_1}\int_0^{S_{1t}/2} Y'(S_1)X'(S_1)dS_1. \end{aligned} \quad (10)$$

Equation (9) can be rearranged to an explicit (non-recursive) relation

$$\alpha_1^{(n)}=(\beta_1)^n, \begin{Bmatrix} \alpha_2^{(n)} \\ \alpha_3^{(n)} \\ \alpha_4^{(n)} \end{Bmatrix} = \left[\sum_{k=1}^{n}\frac{(\beta_1)^{n-k}}{\eta^{2k-2}}\begin{Bmatrix} \beta_1-\beta_5 & \beta_5 & -\beta_6 \\ \beta_5 & \beta_1-\beta_5 & \beta_6 \\ 2\beta_6 & -2\beta_6 & \beta_1-2\beta_5 \end{Bmatrix}^{k-1}\right] \begin{Bmatrix} \beta_2 \\ \beta_3 \\ \beta_4 \end{Bmatrix}. \quad (11)$$

For relatively large size increase $\eta \gg 1$ at each fractal order, the above equation can be significantly simplified to

$$\left\{\alpha_1^{(n)},\alpha_2^{(n)},\alpha_3^{(n)},\alpha_4^{(n)}\right\} \approx (\beta_1)^{n-1}\{\beta_1,\beta_2,\beta_3,\beta_4\}. \quad (12)$$

A fractal shape at each order can be given in the Cartesian coordinates $Y=Y(X)$, such as $Y=-(H_1/2)\sin(2\pi X/L_1)(-L_1/2\le X\le L_1/2)$ for the sinusoidal shape in Figure 1b, where H_1 is the apparent height of the order-1 representative element (Figure 2b). The dimensionless shape parameters are expressed as

$$\begin{aligned} \beta_1 &= \frac{2}{L_1}\int_0^{L_1/2}\sqrt{1+(dY/dX)^2}\,dX, \\ \beta_2 &= \frac{2}{L_1^3}\int_0^{L_1/2}\left[Y(X)\right]^2\sqrt{1+(dY/dX)^2}\,dX, \\ \beta_3 &= \frac{2}{L_1^3}\int_0^{L_1/2}X^2\sqrt{1+(dY/dX)^2}\,dX, \\ \beta_4 &= \frac{-4}{L_1^3}\int_0^{L_1/2}XY(X)\sqrt{1+(dY/dX)^2}\,dX, \\ \beta_5 &= \frac{2}{L_1}\int_0^{L_1/2}\frac{(dY/dX)^2}{\sqrt{1+(dY/dX)^2}}dX, \\ \beta_6 &= \frac{2}{L_1}\int_0^{L_1/2}\frac{dY/dX}{\sqrt{1+(dY/dX)^2}}dX, \end{aligned} \quad (13)$$

where β_1 is the ratio of total length to apparent length, and all other shape parameters depend only on β_1 for each given fractal shape. For example, for the zigzag shape in Figure 1a, .

For an order-n fractal interconnect between two active device islands with the spacing L, the tensile stiffness for a representative element of apparent length L is given by

$$K^{(n)}=\frac{\overline{EI}}{L^3}\frac{4\alpha_3^{(n)}}{4\alpha_2^{(n)}\alpha_3^{(n)}-\left[\alpha_4^{(n)}\right]^2}. \quad (14)$$

For relatively large size increase $\eta \gg 1$ at each fractal order, substitution of Equation (12) gives

$$K^{(n)} \approx \frac{\overline{EI}}{L^3}\frac{1}{\beta_1^{n-1}\left(\beta_2-\frac{\beta_4^2}{4\beta_3}\right)} \quad (15)$$

to be independent of η. It decreases as the fractal order n increase (because $\beta_1>1$), and depends on the fractal shape through $\beta_1^{n-1}\left[\beta_2-\beta_4^2/\beta_4^2/(4\beta_3)\right]$. Here β_2, β_3 and β_4 all depend only on the β_1 for each fractal shape. For example, $\beta_1^{n-1}\left[\beta_2-\beta_4^2/(4\beta_3)\right]$ becomes $7\beta_1^n\left(\beta_1^2-1\right)/768$ for the

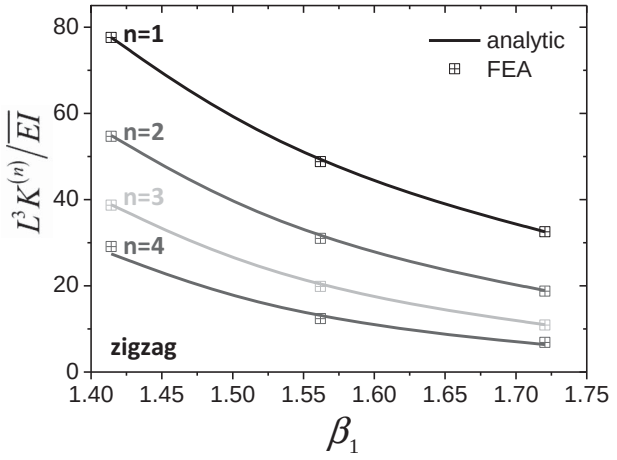

Figure 3. The normalized tensile stiffness $L^3K^{(n)}/\overline{EI}$ versus the ratio of total length to apparent length β_1 for the zigzag fractal shape with the fractal order n ranging from 1 to 4. Results from the analytic model and FEA agree very well.

zigzag shape. **Figure 3** shows the normalized tensile stiffness $L^3K^{(n)}/\overline{EI}$ versus the ratio of total length to apparent length β_1 for the zigzag fractal shape with the fractal order n ranging from 1 to 4. It is clear that the fractal interconnect becomes more compliant as the fractal order n or the total length (represented by β_1) increases. The tensile stiffness is validated by the finite element analysis (FEA). The numerical results shown in Figure 3 for the size ratio $\eta = 10$ across each order agree well with Equation (15). The normalized tensile stiffness for the zigzag, sinusoidal and serpentine fractal shapes and the fractal order $n = 2$ in **Figure 4** suggests that, for the same ratio of total length to apparent length β_1, the dependence on these three shapes is relatively weak.

3. Experiments and Concluding Remarks

Experiments were performed to examine the deformation in a representative fractal interconnect structure. **Figure 5** shows micrographs collected at the original and stretched states of a Cu trace cut by laser milling; the cross sectional dimensions of the trace are 60 μm×60 μm and the apparent length is 4 mm. The interconnect is not adhered to a substrate except its ends, sometimes referred to as 'free-standing'.[20] Stretching of each fractal shape was repeated 3~5 times and all the data points are plotted together to compare with theoretical predictions. Figure 5 also shows the measured force versus nominal strain for zigzag, sinusoidal and serpentine fractal shapes, which agrees well with the analytic model in Section 2 without any parameter fitting. Here the nominal strain is defined as the ratio of the stretched displacement to the apparent length L of the interconnect. The small deviations between experiments and analytical predictions may result from the equipment's limited capability to accurately dictate very small forces (<10 mN). The repeating measurement of stretching verified the repeatability and robustness of the measurements.

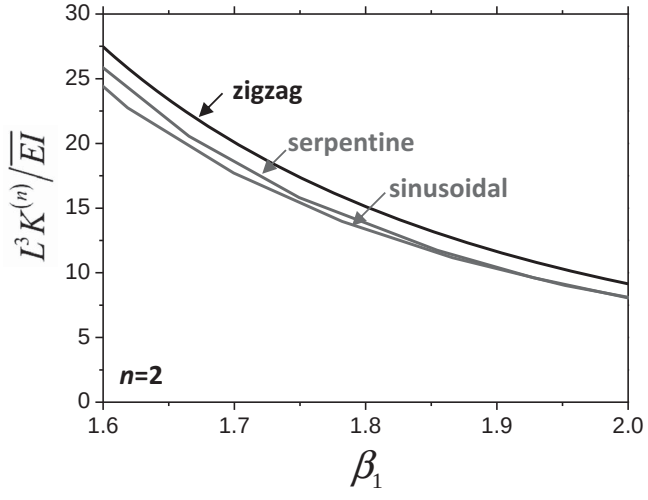

Figure 4. The normalized tensile stiffness for the zigzag, sinusoidal and serpentine fractal shapes and the fractal order $n = 2$.

In summary, the fractal-inspired geometric designs presented in this study provide both key features that are contradicting in most of the other stretchable electronics designs: large stretchability and high aerial coverage of active devices. An analytic method is developed to determine the tensile stiffness of fractal interconnects of arbitrary order n and in arbitrary shape; the tensile stiffness is clearly expressed by a set of non-dimensional parameters; experimental measurements in tensile stiffness agree very well with the analytic predictions.

The fractal interconnects, in general, are much longer than the straight one, which leads to undesired increase in the electric resistance. This can be overcome by using a larger cross section of the interconnects, for which the elastic stiffness is particularly important because their deformation modes tend to be in-plane bending instead of buckling. It is helpful to avoid interfacial peeling under stretching as well.[21,22]

4. Experimental Section

Fabrication of the Fractal Structures: Copper foils (Annealed Alloy 110, Electro Tough Pitch, smooth finish on both sides, All Foils Inc.) were laminated against a flat surface using water soluble tape (3M). A laser milling machine was used to cut out the different traces precisely defined by a CAD file. An infrared (wavelength 790~820 nm) laser beam with a power of 0.10 Watt runs 3 passes along the exterior of the defined edges at a speed of 2.0 mm s^{-1} to cut vertically through the copper foil. Excessive material was removed after the laser milling and the desired traces were left on the flat water-soluble tape for ease of handling.

Testing of Force–Displacement Curve for the Fractal Structures: The water-soluble tape on the clamping pads (squares connected to the ends of the traces, Figure 5) was removed first and then the pads were clamped onto the film-tension clamps of a Dynamic Mechanical Analyzer (Q800, TA Instruments). The backing soluble tape was then dissolved. The fractal traces were

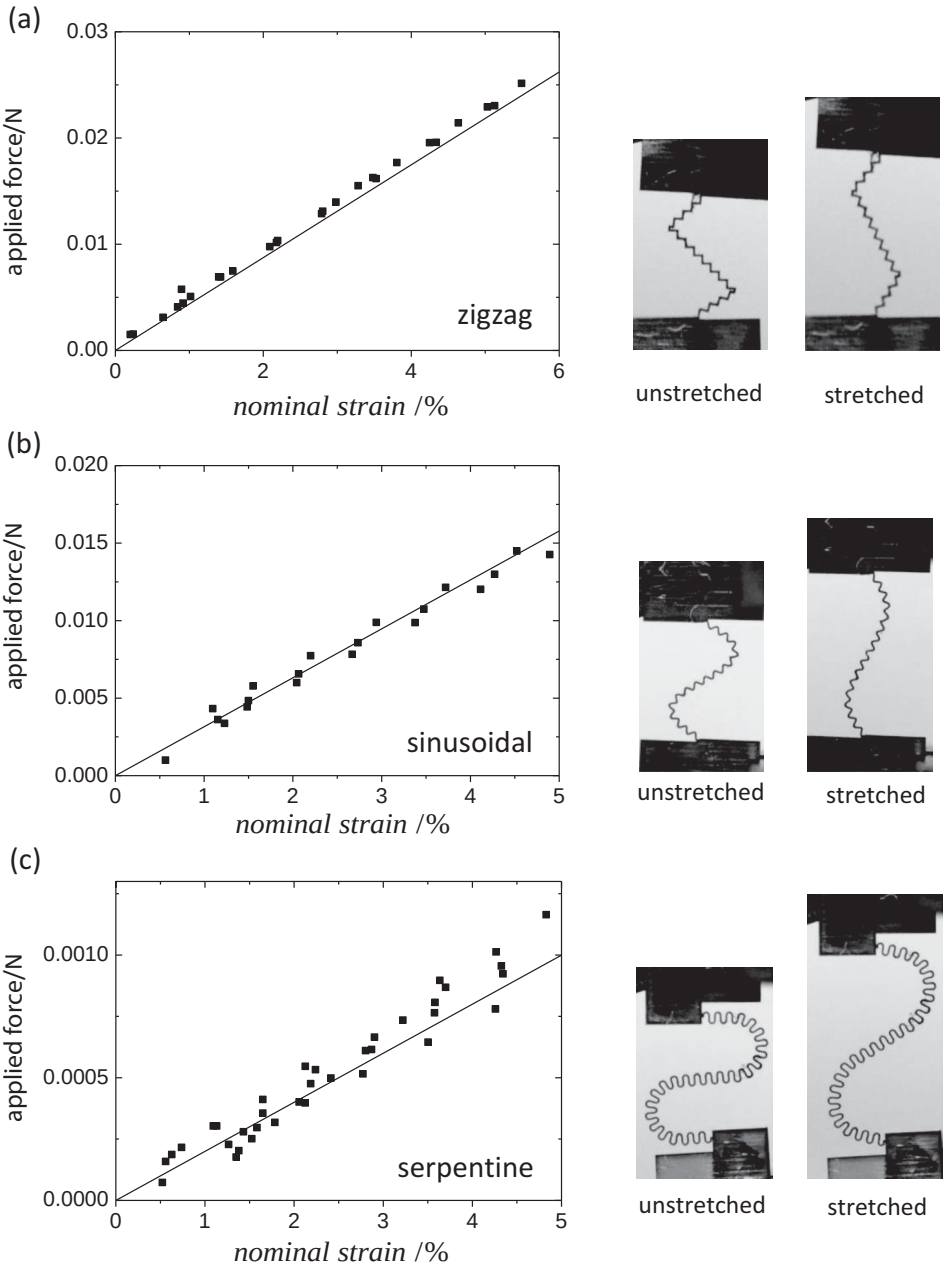

Figure 5. Comparison between the experimental (repeated 3~5 times for each fractal shape) and analytic force-nominal strain curves and the optical microscope images for undeformed and deformed interconnects for the (a) zigzag, (b) sinusoidal and (c) serpentine fractal shapes of fractal order $n = 2$.

stretched at a rate of 0.05 mm s^{-1} while forces were recorded every 2 seconds.

Acknowledgements

Y. Su, S. Wang, and Y. Huang contributed equally to this work. YongAn Huang acknowledges the support from the National Natural Science Foundation of China (51175209).

[1] T. Someya, *Stretchable Electronics*, Wiley-VCH, Weinheim Germany **2013**.
[2] J. A. Rogers, T. Someya, Y. Huang, *Science* **2010**, *327* (5973), 1603–1607.
[3] D. Y. Khang, H. Q. Jiang, Y. Huang, J. A. Rogers, *Science* **2006**, *311* (5758), 208–212.
[4] T. Someya, T. Sekitani, S. Iba, Y. Kato, H. Kawaguchi, T. Sakurai, *Proc. Natl. Acad. Sci. USA* **2004**, *101* (27), 9966–9970.
[5] J. Lee, J. Wu, M. Shi, J. Yoon, S. I. Park, M. Li, Z. Liu, Y. Huang, J. A. Rogers, *Adv. Mater.* **2011**, *23* (8), 986–991.
[6] R. Tang, H. Huang, H. Tu, H. Liang, M. Liang, Z. Song, Y. Xu, H. Jiang, H. Yu, *Appl. Phys. Lett.* **2014**, *104* (8), 083501 .

[7] F. Axisa, P. M. Schmitt, C. Gehin, G. Delhomme, E. McAdams, A. Dittmar, *IEEE T. Inf. Technol. B* **2005**, *9* (3), 325–336.
[8] C. Dagdeviren, S.-W. Hwang, Y. Su, S. Kim, H. Cheng, O. Gur, R. Haney, F. G. Omenetto, Y. Huang, J. A. Rogers, *Small* **2013**, *9* (20), 3398–3404.
[9] D. H. Kim, N. S. Lu, R. Ma, Y. S. Kim, R. H. Kim, S. D. Wang, J. Wu, S. M. Won, H. Tao, A. Islam, K. J. Yu, T. I. Kim, R. Chowdhury, M. Ying, L. Z. Xu, M. Li, H. J. Chung, H. Keum, M. McCormick, P. Liu, Y. W. Zhang, F. G. Omenetto, Y. G. Huang, T. Coleman, J. A. Rogers, *Science* **2011**, *333* (6044), 838–843.
[10] J. Viventi, D. H. Kim, J. D. Moss, Y. S. Kim, J. A. Blanco, N. Annetta, A. Hicks, J. L. Xiao, Y. G. Huang, D. J. Callans, J. A. Rogers, B. Litt, *Sci. Transl. Med.* **2010**, *2* (24), 24ra22 .
[11] H. C. Ko, M. P. Stoykovich, J. Z. Song, V. Malyarchuk, W. M. Choi, C. J. Yu, J. B. Geddes, J. L. Xiao, S. D. Wang, Y. G. Huang, J. A. Rogers, *Nature* **2008**, *454* (7205), 748–753.
[12] J. Vanfleteren, M. Gonzalez, F. Bossuyt, Y. Y. Hsu, T. Vervust, I. De Wolf, M. Jablonski, *MRS Bull.* **2012**, *37* (3), 254–260.
[13] J. A. Rogers, T. Someya, Y. G. Huang, *Science* **2010**, *327* (5973), 1603–1607.
[14] A. Lazarus, J. T. Miller, P. M. Reis, *J. Mechanics Phys. Solids* **2013**, *61* (8), 1712–1736.
[15] Y.-Y. Hsu, M. Gonzalez, F. Bossuyt, J. Vanfleteren, I. De Wolf, *IEEE Trans. Electron Devices* **2011**, *58* (8), 2680–2688.
[16] S. P. Lacour, J. Jones, S. Wagner, T. Li, Z. G. Suo, *Proc. IEEE* **2005**, *93* (8), 1459–1467.
[17] T. Li, Z. Y. Huang, Z. Suo, S. P. Lacour, S. Wagner, *Appl. Phys. Lett.* **2004**, *85* (16), 3435–3437.
[18] S. Xu, Y. Zhang, J. Cho, J. Lee, X. Huang, L. Jia, J. A. Fan, Y. Su, J. Su, H. Zhang, H. Cheng, B. Lu, C. Yu, C. Chuang, T.-i. Kim, T. Song, K. Shigeta, S. Kang, C. Dagdeviren, I. Petrov, P. V. Braun, Y. Huang, U. Paik, J. A. Rogers, *Nat. Commun.* **2013**, *4*, 1543.
[19] J. A. Fan, W.-H. Yeo, Y. Su, Y. Hattori, W. Lee, S.-Y. Jung, Y. Zhang, Z. Liu, H. Cheng, L. Falgout, M. Bajema, T. Coleman, D. Gregoire, R. J. Larsen, Y. Huang, J. A. Rogers, *Nature Commun.* **2014**, *5*, 3266.
[20] D.-H. Kim, J. Song, W. M. Choi, H.-S. Kim, R.-H. Kim, Z. Liu, Y. Y. Huang, K.-C. Hwang, Y. Zhang, J. A. Rogers, *Proc. Natl. Acad. Sci. USA* **2008**, *105* (48), 18675–18680.
[21] Y.-Y. Hsu, M. Gonzalez, F. Bossuyt, F. Axisa, J. Vanfleteren, I. De Wolf, *J. Mater. Res.* **2009**, *24* (12), 3573–3582.
[22] Y. Duan, Y. Huang, Z. Yin, N. Bu, W. Dong, *Nanoscale* **2014**, *6* (6), 3289–3295.

Received: April 29, 2014
Revised: June 23, 2014
Published online: September 2, 2014